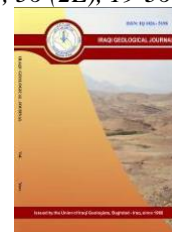




# Iraqi Geological Journal

Journal homepage: <https://www.igi-iraq.org>



## Petrographical and Geochemical Features of Sulfide Mineralization in the Walash Group, Gallala Area, Kurdistan Region of Iraq

Twana A. Mustafa<sup>1\*</sup>, Tola A. Mirza<sup>1</sup> and Stavros P. Kalaitzidis<sup>2</sup>

1 Department of Geology, College of Science, University of Sulaimani, Sulaimani, Kurdistan Region. Iraq

2 Department of Geology, University of Patras, Gr-26504 Rio Patras. Greece

\* Correspondence: [twana.ahmed@uor.edu.krd](mailto:twana.ahmed@uor.edu.krd)

Received:  
20 June 2023

Accepted:  
7 August 2023

Published:  
30 November 2023

### Abstract

In this article, a Fe-rich sulfide mineralization hosted within the Walash Group in the Gallala area, on the northwestern side of the Zagros Orogen is investigated for the first time. The mineralization occurs as massive sulfide veins and veinlets, as well as disseminated within volcanic lithologies. The objective of the study is to characterize the sulfide-rich mineralization using petrographical and geochemical methods, applied in both the ores and the corresponding host formations, including the characterization of volcanic rock alteration. Petrographic data indicates the presence of Fe-rich sulfide mineralization in altered basaltic andesite to andesite rocks, which are affected by hydrothermal alteration such as actinolization, chloritization, sericitization, and epidotization. The geochemical analysis of the fresh rock samples reveals enrichment of iron in the suture zones, but low copper and zinc concentrations. The mineralogical and textural signatures of sulfide minerals lead to inferring that the ore mineralization origin is volcanogenic to the hydrothermal type of deposits.

**Keywords:** Gallala area; Hydrothermal alteration; Sulfide Mineralization; Walash Group; Volcanogenic; Hydrothermal origin

### 1. Introduction

The Gallala sulfide mineralization is located in the Kurdistan Region of Iraq (KRI), close to the Iranian border, approximately 150 kilometers from the Erbil governorate, and at an altitude between +1600m and +1800m (Fig. 1a, and b). Stratigraphically the studied area belongs to the Walash-Naopurdan Group, which contains an extended distribution of ultramafic, mafic, and volcano-sedimentary rocks (Fig. 2), including a wide variety of mineral resources. These mineral resources are hosted by intermediate volcanic and sedimentary rocks, including pyroclastic flows that are well-developed in the Zagros Suture Zones (ZSZ) and belong to the northeastern part of the Zagros Orogen. During the 1960s, the broader area was explored by Technoexport from Russia in collaboration with the Iraqi Geological Survey, which focused its work on the Kurdistan Region, especially in the Rawanduz district (Gallala, Kawarta, Darband, and Rayat). Based on their work, several chromites and sulfide mineralizations were discovered, and the map has been revised by providing more accurate structural and stratigraphic descriptions (Al-Bassam, 2013).

The recrystallization and destruction of primary textures during post-ore deformation and metamorphism restrict the comprehension of the genetic history of many old volcanogenic massive sulfide (VMS) deposits (Marshall and Gilligan, 1993). Nevertheless, the primary textures are preserved

DOI: [10.46717/igi.56.2E.2ms-2023-11-7](https://doi.org/10.46717/igi.56.2E.2ms-2023-11-7)

in several Mesozoic and Cenozoic VMS deposits, including those in Cyprus (Oudin and Constantinou, 1984, Adamides, 2010), Japan (Eldridge et al., 1983), Oman (Haymon et al., 1984), Maine, USA (Slack et al., 2003), and Altai-Sayan region, Russia (Simonov et al., 2010), a fact that allowed the building up of genetic models.

There is a relatively known VMS deposit along the Zagros Orogenic Belt (ZOB), this of Sargaz deposits in southeast Iran, that is one of the least distorted and metamorphosed of the ZOB (Badrzadeh et al., 2011). The prospecting area for VMS mineralization in the Kurdistan Region is situated within the Zagros Suture Zone, a slightly arched tecto-magmatic belt of the Walsh volcanic rocks in the Mawat ophiolite; they are encompassed by basic to acidic igneous intrusions with a prevalent mineral alteration process (Palinkas and Mirza, 2020).



**Fig. 1.** a: Iraqi map with neighbor countries, showing the studied area b: Satellite image of northeast Iraq (Kurdistan Region) showing the location of the Gallala sub-district (from Google Earth)

There are a variety of investigations for prospecting of various minerals conducted by Al-Chalabi (2004), Jassim and Goff (2006), Ismail and Al-Chalabi (2006), Ismail et al. (2009), Ahmed et al. (2020), Pirouei et al. (2021), and Pirouei et al. (2022), who reported that chromite and iron oxide mineralization along sulfides occurs within the Walsh-Naopurdan Group, especially at the nearby Rayat area. Moreover, Aziz (2008), and Ali et al. (2013) studied the petrographic and geochemical aspects of the rocks that covered the Gallala area.

This study focuses on the characterization of sulfide mineralization in the Gallala area, which crops out within the Walsh volcano-sedimentary rocks. New data related to the geological, petrographical, and geochemical features of their host rocks are presented to provide initial insights towards interpreting the characteristics and genesis of the sulfide mineralization.

## 2. Tectonic and Geological Setting

The exposed host rocks of the studied area belong to the Walsh-Naopurdan volcano-sedimentary Group (Jassim and Goff, 2006), which is part of the Zagros Orogenic Belt. The Zagros Orogenic Belt is a result of the closure of Neo Tethys between Arabian and Iranian microplates through the convergence of the African Gondwanian and Eurasian continental blocks (Alavi and Mahdavi, 1994). The Cenozoic

Zagros continent-continent collision took place from the Eocene to the Miocene (Agard et al., 2011, Zhang et al., 2017, Barber et al., 2018, Koshnaw et al., 2021).

The western part of the Zagros Fold and Thrust Belt of Iraq is classified by Fouad (2015) into four parallel architectural zones: Low Folded Zone, High Folded Zone, Imbricate Zone, and Suture Zone (Fig. 2a). The Iraqi Zagros Suture Zone (IZSZ) is subdivided into two main tectonic Subzones: Qulqula–Khwakurk Subzone and Penjween Walsh Subzone (Zainy et al., 2017).

The Penjween-Walash Subzone is distinguished by two allochthonous thrust sheets, which are designated by the upper and lower thrust sheets (Aswad, 1999, Aswad et al., 2011) (Fig. 2b). The Upper Allochthonous composed of ophiolite-bearing terrane integrated of Mawat Ophiolitic Massif of Albian-Cenomenian (97-105 Ma) and Gimo-Qandil sequence, whereas the volcano-sedimentary rocks of the Walsh-Naopurdan nappe are referred to the Lower Allochthonous sheet (Aswad and Elias, 1988) (Fig. 2b). The Cretaceous ophiolite and supra subduction zone complexes are part of the Qandil Sheet, which is incorporated by the Bulfat, Mawat, Penjween, and Pushtashan episodes (Ismail et al., 2014) (Fig. 2c). The Walsh-Naopurdan Group refers to the back-arc, calc-alkaline, and alkaline suites for the Walsh rocks, while the Naopurdan rocks are related to the island-arc tholeiitic suite (Ali, 2012). Stratigraphically, the Walsh Group was nominated for an Eocene-Oligocene age depending on, the recent radiometric dating of the basaltic rocks (Ali et al., 2013).

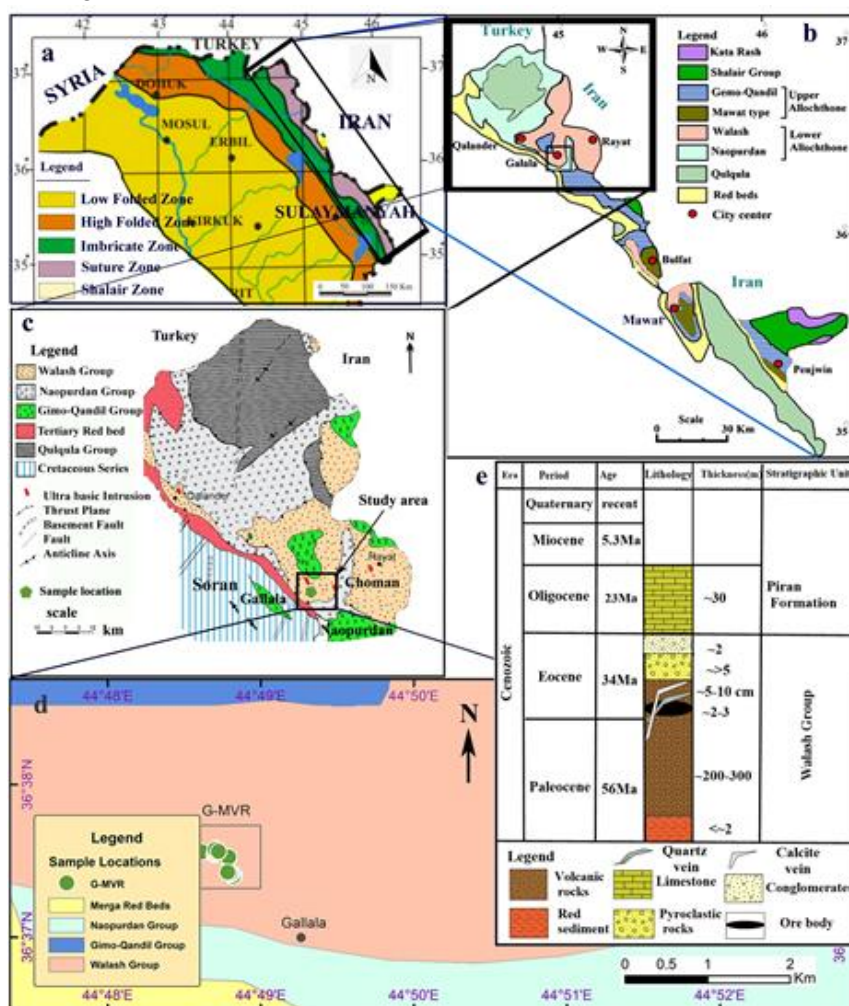


**Fig. 2.** A) Tectonic subdivisions of Northeastern Iraq (Fouad, 2015) b) Simplified Geological map of the Zagros Suture Zone (Jassim et al., 1982, Aswad et al., 2014) c) Geological map of northeastern Iraq, showing the location of Gallala area (Modified from Buday (1980)), in Ali et al. (2013) d) Geological map of the study area e) Lithostratigraphic columnar section of the Walsh Group in the studied area.

The Metallogenic Province of the ZSZ is distinct by ore mineral formations during the Cretaceous and Paleogene periods. The process of mineral formations is referred genetically to the magmatic, volcanic, metamorphic, and hydrothermal processes, which are pertained to the tectonism through the convergence between Arabian and Iranian microplates within the suture of the Neo-Tethys (Jassim and Goff, 2006, Al-Bassam, 2013).

The Penjween-Walash Subzone is the prominent metallogenic region of North-eastern Iraq, with abundant metallic ore minerals of magmatic and hydrothermal origin. In addition, Cu and Fe mineralization in the Walash-Naopurdan Groups represents ore formations that originated via Paleogene magmatism of the Zagros Suture Zone (Al-Bassam, 2013). Iron, copper, and zinc are the abundant metallic minerals that build up the main sulfide mineralization of the study area.

The Walash Group includes volcanic lithologies, while the sedimentary rocks within the extrusive volcanic rocks are texturally immature and consist of red mudstone, cherty siltstone, red and grey shales, greywackes, conglomerates, radiolarian chert, tuffs, and limestones, whereas the sedimentary rocks of the Naopurdan Group consist of slates, shales, sandstones, nummulitic limestone and conglomerate with basic volcanic clasts (Buday, 1980, Jassim and Goff, 2006).

The volcanic rocks in the Walash Group are classified into basic dykes, lava flows, pillow lavas, (generally spilitic diabase and pyroxene-bearing spilitic basalt and spilite) and intermediate volcanics (pyroxene andesite, pyroxene-amphibole andesite, amphibole andesite and altered andesite, and pyroclastic rocks intercalated with sediments) (Jassim and Goff, 2006). Stratigraphically the studied section is composed of volcanic rocks associated with red sediments; along fracture zones, these rocks contain sulfide ore mineralization (Fig.2e).

Regional mapping showed that the andesitic rocks in the Gallala Middle Volcanic Rock section (G-MVR) cover the northwest part of the Gallala sub-district, which is the host of the sulfide mineralization. The dominant country rocks consist of volcanic rocks that are grayish, green to brownish-gray volcanic rocks, and are characterized by massive, fractured to brecciated texture, cross-cut by quartz and calcite veins (Figs. 3 a, b, c, and d). The volcanic rocks are overlain by conglomerates and pyroclastic materials (Figs. 3 e and f). The red siliceous carbonates form patches or lenses intertwining with the igneous host rocks (Fig. 3g). In addition, 2 m thick and more than 1 km long red radiolarian cherts are associated with the volcanic rocks (Fig. 3h).

The sulfide mineralization of the Gallala area occurs in two textural types: (I) disseminated within the host rocks, and (ii) massive sulfide veins and veinlets. The disseminated sulfide mineralization has been estimated from 350 to 400 m in length and 2 to 3 m in thickness (Fig. 4a, and b), whereas the massive vein-type ore mineralization occurs as 1.5 to 2 m long, and 10 to 15 cm thick veins, (Fig. 4c, d, e, and f). Additionally, barren quartz veins up to 10 cm thickness cross-cut the host rocks in several places (Fig. 4a). Weathering surface of the host rocks such as limonitization and malachite staining on the volcanic rocks are the pathway traces for the sulfide mineralization in the studied area (Figs. 4g, and h). In addition, pyrite represents the major sulfide ore mineralization, identified macroscopically in the G-MVR location.

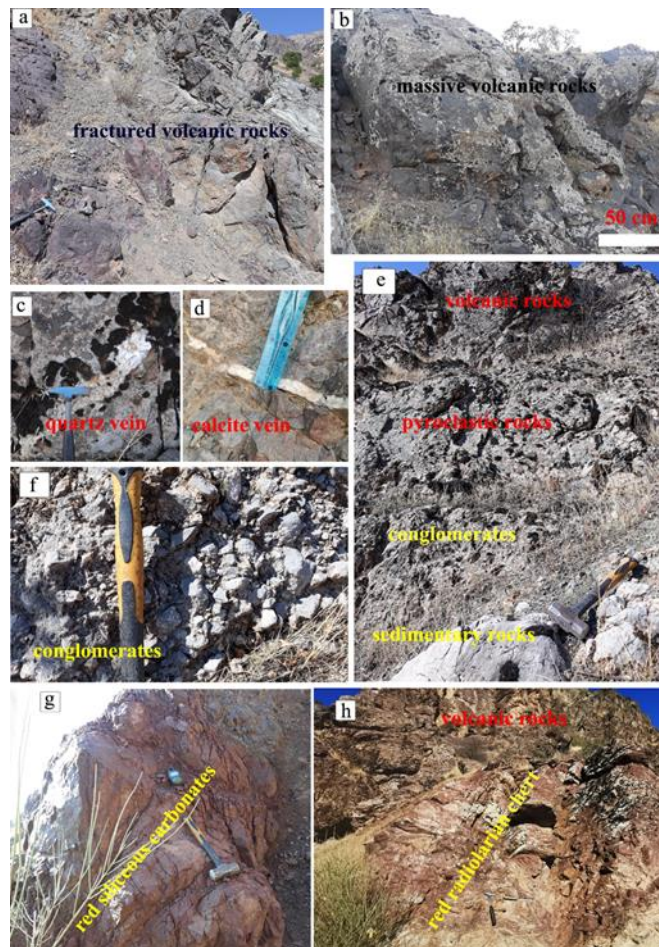


**Fig. 3.** The rock constituents of the MVR are present at the G-MVR location. a: Red to grayish-green, fractured and brecciated volcanic rocks; b: Massive volcanic rocks; c & d: Quartz and calcite veins within the volcanic rocks; e: Volcanic rocks associated with pyroclastic and sedimentary rocks; g: Patches and lenses of red siliceous carbonate rocks; h: Association of the red radiolarian chert along volcanic rocks

### 3. Materials and Methods

Thirty samples were collected from the surface of igneous bodies in several out-crops of the Walsh Group in the Gallala area, including 10 samples of host rocks, and 20 of mineralization. Twenty thin sections and ten polished blocks were prepared at Kurdistan Institution for Strategic Studies and Scientific Research (KISSR). Thin sections were used for petrographic observation by using a transmitted light polarizing microscope to ascertain textures and mineral identifications. Additionally, polished sections were prepared from the sulfide ores and studied by using a Meiji transmitted and reflected light microscope at the Department of Geology, College of Science, University of Sulaimani. Microscopic studies of the ore samples aimed to obtain their mineralogy, texture, and microstructural characteristics.

Mineralogical analysis was performed for twelve volcanic host rocks with sulfide ore samples using a Burker D8 Advance X-ray diffractometer (XRD) equipped with a Lynx-Eye® detector. The

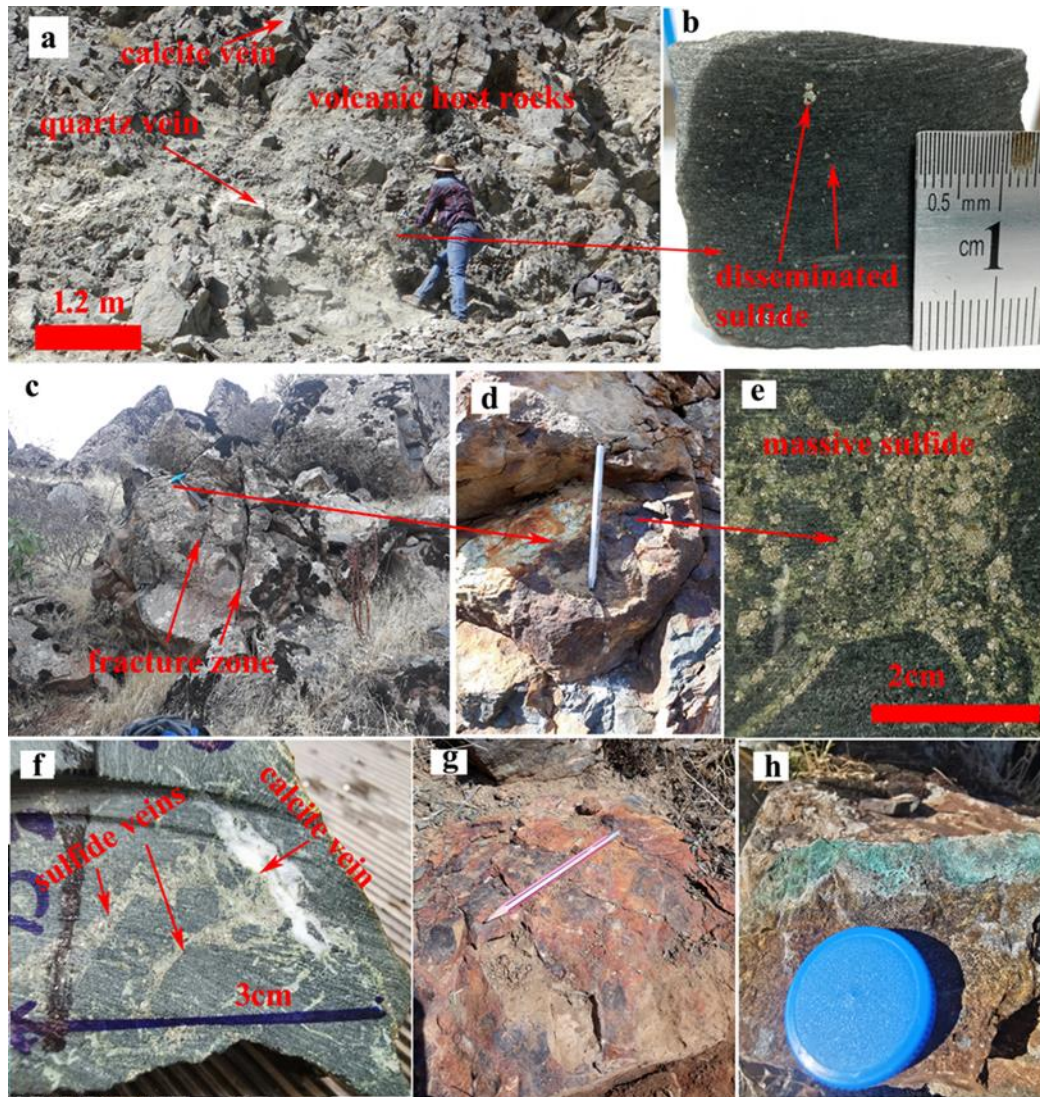


**Fig. 4.** The ore features of the MVR at the G-MVR location. a: Disseminated sulfide mineralization hosted by volcanic rocks being crosscut by quartz veins; b: Disseminated sulfides; c: Fractures of the volcanic rocks hosting massive vein sulfides; d: Ore mineralization within the lava complex; e: Mineralization with massive vein sulfides; f: Sulfides and calcite veins; g: Weathered surface of the host rocks; h: Malachite staining on the rock surface

scanning area covered the interval  $2\theta$  4-70°, with a scanning angle step of 0.015° and a time step of 1 s. The identification of mineral phases was attained by using EVA® software; the mineral contents were semi-quantitatively determined using the Rietveld-based TOPAS® software and applying the technique described in detail by Siavalas et al. (2009). The XRD analysis was carried out at the facilities of the Section of Earth Materials, University of Patras, Greece. In addition, major and trace element compositions of the studied samples were examined by using X-Ray fluorescence. Fifteen samples of the volcanic host rocks were selected and each of them was powdered through a 200 mesh in an agate mill to avoid contamination. Fused glass discs were prepared for major element analysis by X-ray fluorescence (XRF) at facilities of the Laboratory of Electron Microscopy and Microanalysis of the Faculty of Natural Science, University of Patras, Greece.

## 4. Results

### 4.1. Petrographical Features of the Host Rocks

The petrographic study of the volcanic rocks based on microscopic observations and X-Ray Diffraction (XRD) data reveals that the mineralogical composition and the percentages of the essential minerals consist of plagioclase (9%-61%), quartz (2% -11%), pyroxene (1%-14%), amphibole (riebeckite) (2%-34%), and opaque minerals (1%- 4%) (Table 1, Fig.5). The opaque minerals of the studied samples appear in the form of phenocrysts, micro phenocrysts, and a groundmass. Additionally, the secondary minerals, including chlorite (4%-19%), prehnite (7%-15%), and clay minerals (1%-11%), manifested as a form of a matrix (Table 1). The mineral compositions correspond to basaltic andesite to andesite rocks, with no distinct megascopic discrimination between the two volcanic rocks in the study area.

**Table 1.** The semi-quantitative mineral contents of the studied area using TOPAZ software (% of the crystalline phases)

Location	Rock type	Mineral contents				Ore minerals	Range %
		Essential	Range %	Accessory	Range %		
G-MVR	15 samples of volcanic rocks hosting oxide and	Pyroxene	1.0-14.0	Opaque	1.0-4.0	Fe-Oxide	1.0-4.0
		Amphibole	2.0-34.0	Chlorite	4.0-19.0		
		Plagioclase	9.0-61.0	Clay minerals	1.0-11.0	Pyrite	1.0-3.5
		Quartz	2.0-11.0	Prehnite	7.0-15.0		

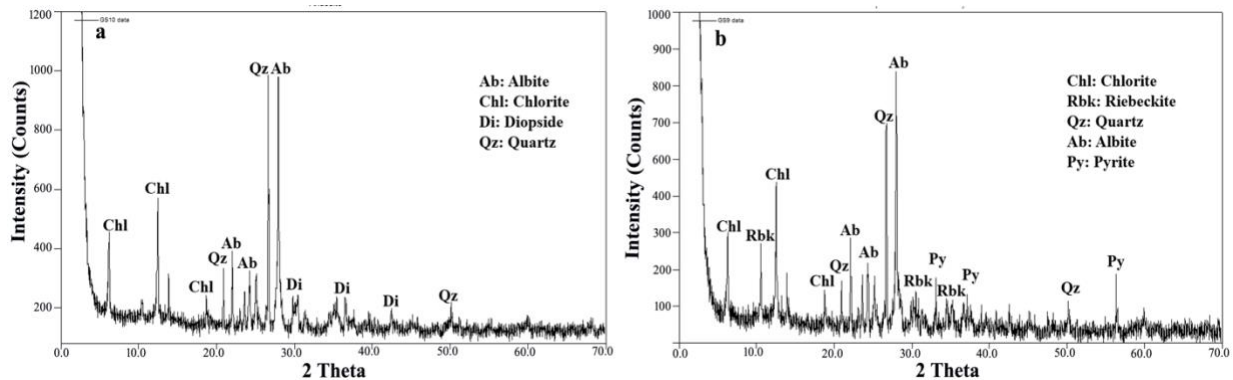


**Fig. 5.** Example of the two Gallala samples XRD diffractograms (minerals abbr. based on Warr (2021))

The crystal framework of volcanic rocks of the study area represents holo-crystalline to hypocrystalline grains with cryptocrystalline groundmass. Felty or pilotaxitic, orthophyric, porphyritic, and intergranular textures are the dominant microstructures of volcanic rocks (Fig. 6). The phenocrysts and micro phenocrysts range from 40-45 vol. %, including plagioclase, clinopyroxene, amphibole (hornblende), and opaque minerals. Moreover, the rest of the ground masses include plagioclase, mafic minerals, and texturally, both phenocrysts and groundmass are coexisting in the rock samples. (Fig. 6).

The pilotaxitic texture is distinguished by the micro-phenocrysts of plagioclase that are randomly oriented within the groundmass (Figs. 6a, and b). The subhedral epidote grains appear on the anhedral opaque grains (Fig. 6c and d). Additionally, the groundmass and microlites designate a flow foliation consisting of plagioclase, opaque minerals, and amphiboles with orthophyric textures along amygdules filled with calcite and quartz (Figs. 6e, and f). However, the phenocrysts and micro phenocrysts are

mainly plagioclase mostly altered to sericite and opaque minerals with hornblende and pyroxene set in a cryptocrystalline groundmass, which is an implication feature of the porphyritic textures (Fig. 6g, and h).

The porphyritic texture is constricted largely to volcanic rocks. It occurs when the magma with its enclosed crystals is abruptly shifted to a higher level in the crust or extruded at the surface (Tyrrell, 2012). The characteristic distribution of the intergranular or interstitial texture reveals the laths of plagioclase crystal embedded by subhedral of clinopyroxene and hornblende grains (Fig. 6i, and j). The mineral assemblage and textural feature of the studied rock samples represent basaltic andesite rocks, and the intermediates are andesite rocks that are associated with red radiolarian chert.

Plagioclase is the most significant felsic mineral constituent in volcanic rocks in the form of conspicuous phenocrysts with abundant groundmass microlites. The plagioclase phenocrysts range from 0.05mm to 0.20mm. Additionally, most plagioclase is albite displaying idiomorphic to sub-idiomorphic crystals (lath-shaped and acicular microlites with swallow tail bifurcation and some of the plagioclase grains exhibit alteration to sericite (Fig. 6 f, h, and j).

Pyroxene and amphiboles are the dominant mafic minerals that occur as idiomorphic to sub-idiomorphic crystals with the size of their phenocrysts ranging from 0.02mm to 0.25mm. Besides, the colorless to weakly pleochroic of the clinopyroxene and the hornblende show strong pleochroism from pale brown to reddish-brown, along with yellowish to strong pleochroic of actinolite (Fig. 6c, d, and j).

Most of the opaque minerals in the studied samples display the euhedral and subhedral to anhedral crystals that are composed of tabular, and brecciated iron-rich sulfide mineralization, and the range of their phenocrysts are between 0.1mm to 0.40mm (Fig. 6).

## 4.2. Ore Petrography

The predominant ore minerals within the volcanic host rocks are Fe-rich sulfides with a minor amount of iron oxides (Fig. 7). The sulfides occur as: (i) fine to medium-sized grains usually disseminated, and(ii) coarse-grained massive vein sulfides comprising assemblages of up to centimeter-sized crystals of pyrite being the most significant type. Additionally, anhedral fine to medium-grained iron oxides (magnetite and pseudomorphs after magnetite; i.e., martite is a variety of hematite) are encountered within the disseminated sulfides. Within the disseminated sulfides, pyrite and subordinate iron oxides such as magnetite and hematite are observed (Fig.7a, b, and c), whereas in the massive sulfide vein-type minor amount of chalcopyrite, bornite, covellite, sphalerite, and pyrrhotite, as well as, malachite is found, as a secondary mineral (Fig.7d, and e). Secondary minerals like limonite and malachite can be observed on the surface of the mineralization areas, indicating that they represent alteration products of the sulfide minerals (Fig.4 g, and h), formed by the weathering and oxidation of the latter

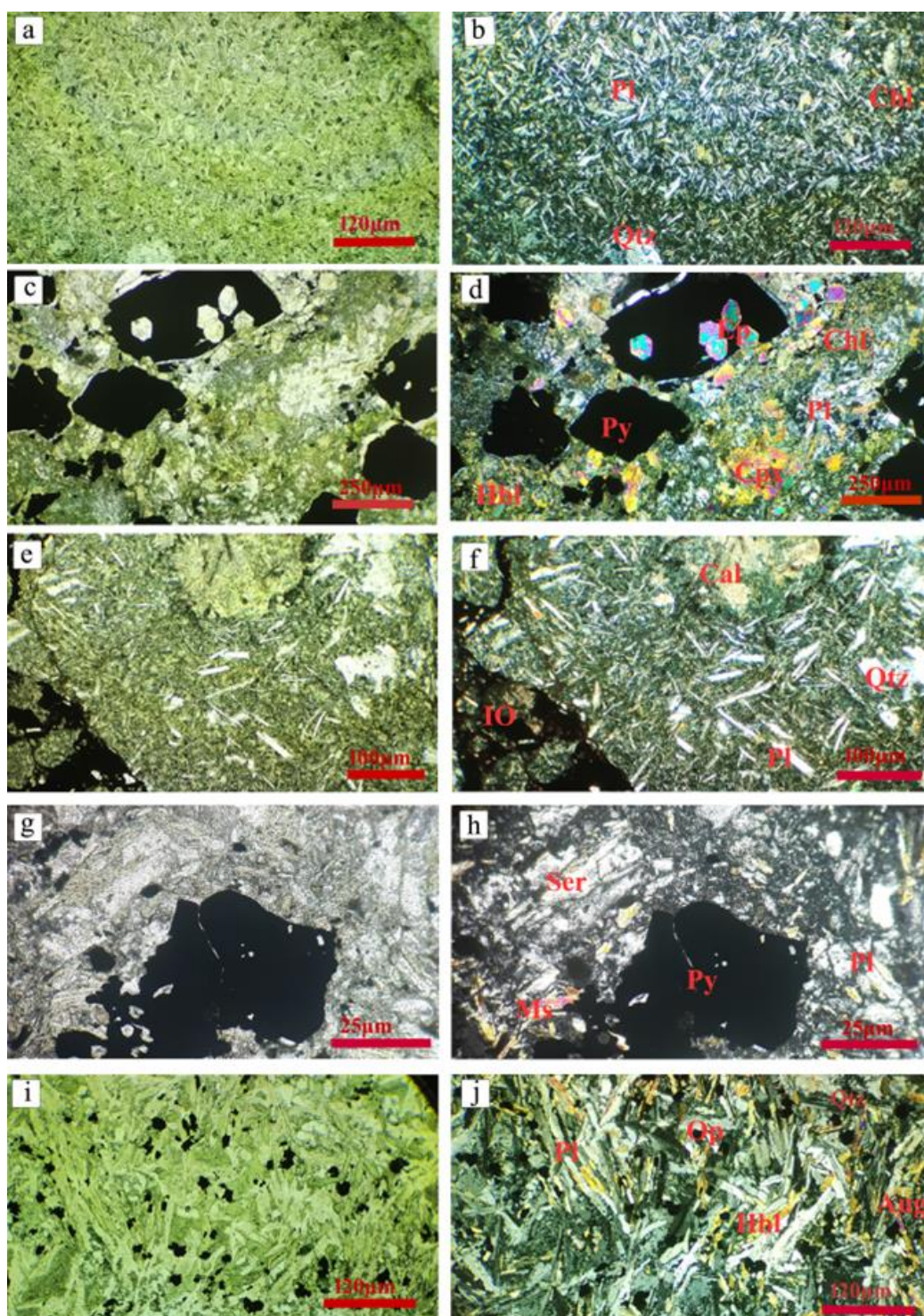


**Fig. 6.** Photomicrographs of the basaltic andesite rocks from the G-MVR location. a and b: Pilotaxitic texture in which the micropenocrysts of plagioclase are randomly oriented X10, PPL, and XPL, respectively; c and d: Epidote inclusions with chlotitization of mafic minerals X10, PPL, and XPL respectively; e and f: Amygdules filled by quartz and calcite in the basaltic ande-site rock X10, PPL and XPL respectively; g and h: Porphyritic texture showing the alteration of plagioclase phenocryst to sericite surrounded by groundmass X20, PPL and XPL respectively; i and j: Intergranular or interstitial texture of andesite that exhibits the lath-shaped plagioclase embedded by augite, actinolite, and opaque minerals X20, PPL and XPL respectively. (Pl: Plagioclase, Chl: Chlorite, Qz: Quartz, Py: Pyrite, Ep: Epidote, Cpx: Clinopyroxene, Hbl: Hornblende, Ser: Sericite, IO: Iron oxide, Aug: Augite, Act: Actinolite, Op: Opaque minerals)

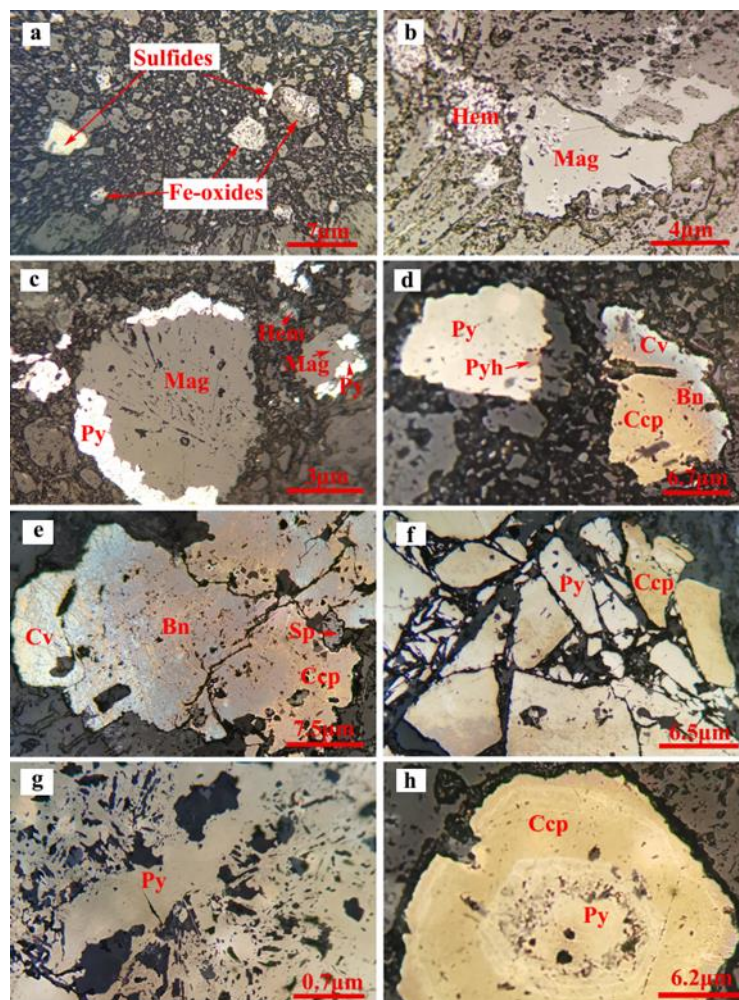


**Fig. 7.** Photomicrographs of G-MVR samples taken under reflected light. a: Disseminated sulfides associated with iron oxides X5, PPL; b: Hematite (martite) replacing magnetite X10, PPL; c: Replacement of magnetite by pyrite X10, PPL; d: Overgrowth of pyrrhotite on pyrite, and the replacement between copper sulfides X10, PPL; e: Replacement of Chalcopyrite by bornite, covellite, and infilling sphalerite X10, PPL; f: Brecciated pyrite and chalcopyrite X10, PPL; g: Sieve texture of pyrite X10, PPL; h: Zonation of pyrite and chalcopyrite X10, PPL (Mag: Magnetite; Pyh: Pyrrhotite; Py: Pyrite; Ccp: Chalcopyrite; Bn: Bornite; Cv: Covellite; Hem: Hematite; Sp: Sphalerite)

Pyrite is the most abundant sulfide coexisting with magnetite, pyrrhotite, chalcopyrite, bornite, covellite, and sphalerite in the studied samples. In general, pyrite is in the form of subhedral to anhedral crystals, whereas magnetite, hematite (martite), chalcopyrite, bornite, and covellite are present as anhedral crystals, with fine spherical disseminated pyrrhotite on pyrite, and sphalerite displays usually irregular forms (Fig.7). Among the disseminated sulfides, magnetite was replaced by pseudomorphs of hematite and Fe-disulfides (pyrrhotite and pyrite) (Fig. 7 a, b, and c). On the other hand, the coarse-grained pyrites were replaced by Cu-Zn-sulfides (Fig. 7d). Furthermore, anhedral chalcopyrite was replaced by bornite and covellite (Fig. 7e). In some instances, pyrrhotite and sphalerite are found to have overgrowth, infilling, and inclusions within pyrite (Figs. 7d, and e). The sulfide minerals are distributed as intergrowths disseminated, and massive; while the predominant textures of these sulfide minerals are replacement, brecciated, sieve, and zonal replacement textures (Fig.7). Quartz, chlorite, sericite, albite, and amphiboles are the most dominant gangue minerals. Moreover, the gangue minerals are distributed as a matrix, representing intergrown silicate minerals between the sulfide ore minerals (Figs. 6 and 7).

### 4.3. Geochemical Features

The data from the geochemical investigation are presented in Table 2. The compositional variations in the major oxide analyses of the selected samples are composed of SiO<sub>2</sub> (53.53-58.02 wt.%), Al<sub>2</sub>O<sub>3</sub> (10.98-13.72 wt.%), Fe<sub>2</sub>O<sub>3</sub> (8.57-13.23 wt.%), CaO (2.59-5.59 wt.%), MgO (4.77-8.93 wt.%), Na<sub>2</sub>O (2.63-5.54 wt.%), K<sub>2</sub>O (0.22-1.42 wt.%), TiO<sub>2</sub> (0.63-1.26 wt.%), MnO (0.20-0.44 wt.%), and P<sub>2</sub>O<sub>5</sub> (0.03-0.08 wt.%). The total alkali contents (Na<sub>2</sub>O+K<sub>2</sub>O) vary from 3.77 wt.% to 6.30 wt.% with an average of 5.05 wt.%.

**Table 2.** XRF geochemical data of the Gallala volcanic host rocks

Sa mp le	MV1	MV2	MV3	MV4	MV5	MV6	MV7	MV8	MV9	MV10	MV11	MV 12
wt												
SiO	55.26	57.62	56.29	56.33	53.53	56.97	53.99	58.02	54.25	55.39	56.23	55.5
Al <sub>2</sub>	11.06	11.80	11.96	12.60	11.71	11.14	10.98	11.68	13.44	13.72	13.20	12.1
Fe <sub>2</sub>	11.62	11.77	8.57	10.80	12.75	12.03	13.23	11.64	12.46	12.72	10.93	12.8
Mn	0.42	0.33	0.28	0.42	0.29	0.44	0.36	0.36	0.20	0.21	0.30	0.23
Mg	7.97	6.57	8.39	6.70	8.93	6.95	7.22	6.73	4.77	4.86	6.93	6.66
Ca	4.35	3.11	5.59	3.06	3.03	2.89	3.65	2.59	3.16	3.23	3.72	2.86
Na <sub>2</sub>	4.11	5.54	2.63	4.57	3.54	4.58	3.88	4.29	5.05	5.15	5.09	3.81
K <sub>2</sub> O	0.35	0.13	1.42	0.89	0.22	0.45	0.28	0.56	1.12	1.15	0.60	1.21
TiO	0.65	0.91	0.63	0.91	1.20	1.19	1.10	1.18	1.06	1.08	0.83	1.26
P <sub>2</sub> O	0.03	0.05	0.06	0.05	0.06	0.06	0.06	0.07	0.05	0.05	0.06	0.08
LOI	3.26	2.27	4.04	3.31	4.57	2.85	4.91	2.93	2.35	2.35	3.19	2.71
Tot	99.08	100.1	99.86	99.65	99.83	99.55	99.67	100.1	97.91	99.91	101.1	99.4
Na <sub>2</sub>	4.46	5.67	4.05	5.47	3.77	5.03	4.16	4.85	6.17	6.30	5.68	5.02
mg/												
Sc	13	14	19	16	24	27	15	15	54	22	19	21
V	262	220	167	226	294	321	271	330	260	155	257	301
Cr	25	16	42	27	28	16	17	16	12	18	16	15
Co	10	9	7	6	9	8	9	7	5	3	7	7
Ni	4	2	42	6	3	2	2	2	3	10	2	2
Cu	1	2	329	24	278	429	57	1	1538	2	99	245
Zn	159	93	116	69	69	233	251	231	142	116	127	105
Rb	<1	<1	24	19	<1	<1	<1	<1	15	<1	<1	2
Sr	90	105	138	230	171	42	153	118	146	163	162	146
Y	31	36	32	45	42	33	30	35	46	53	45	45
Zr	18	29	26	37	36	30	32	33	44	19	38	39
Nb	0.3	0.4	0.8	0.3	0.8	1	0.5	0.5	0.3	1	0.7	0.7
Ba	91	95	212	176	75	49	83	114	67	123	129	126
Hf	4	5	28	5	0	38	3	4	263	<1	10	1
Pb	2	3	4	5	2	2	4	1	2	<1	3	<1
La	1	1	2	2	1	2	1	1	1	2	1	1
Ce	7	8	15	14	10	8	6	9	10	<1	9	12
Yb	2	2	3	3	2	2	2	3	3	3	3	2
Th	1	<1	2	1	1	<1	1	1	<1	<1	<1	1
Zr/	28	32	41	40	30	25	29	28	42	17	46	31
Nb/	0.3	0.4	0.4	0.2	0.9	1	0.5	0.5	0.3	0.6	0.7	0.71
La/	0.5	0.5	0.7	0.7	0.5	0.5	0.5	0.3	0.3	0.6	0.3	0.5

The loss-on ignition in the studied samples ranged from 2.27 wt.% to 4.91 wt.%, showing a fluid-assisted alteration process and low-grade metamorphism (Ural et al., 2015). Regarding the trace element compositions of the studied samples, copper, zinc, vanadium, barium, and strontium display high concentrations in the igneous bodies (Table 2). The highest contents of chalcophile elements are Cu and Zn, ranging from 1-1538 mg/kg, and 69-251 mg/kg, respectively, with low Pb content <1 to 4 mg/kg,

whereas Ba is recorded in the MV samples with contents from 49 to 212 mg/kg. On the other hand, nickel, chrome, and zircon display low concentrations in the Gallala samples.

## 5. Discussion

### 5.1. Nature of the Volcanic Host Rocks

The total alkali versus silica (TAS) diagram Le Bas et al. (1992), and Middlemost (1994) are used for the geochemical classification of the Gallala volcanic host rocks; the studied samples are plotted in the field of basaltic andesite to andesite rocks, with one sample being plotted in the trachy-andesite field. The overall data indicate that the volcanic rocks have sub-alkaline affinity (Fig. 8a, and b). Furthermore, by applying the Zr/TiO<sub>2</sub> versus SiO<sub>2</sub> diagram of Winchester and Floyd (1977) the volcanic rocks of the Gallala area are plotted in the andesite domain (Fig. 8c).

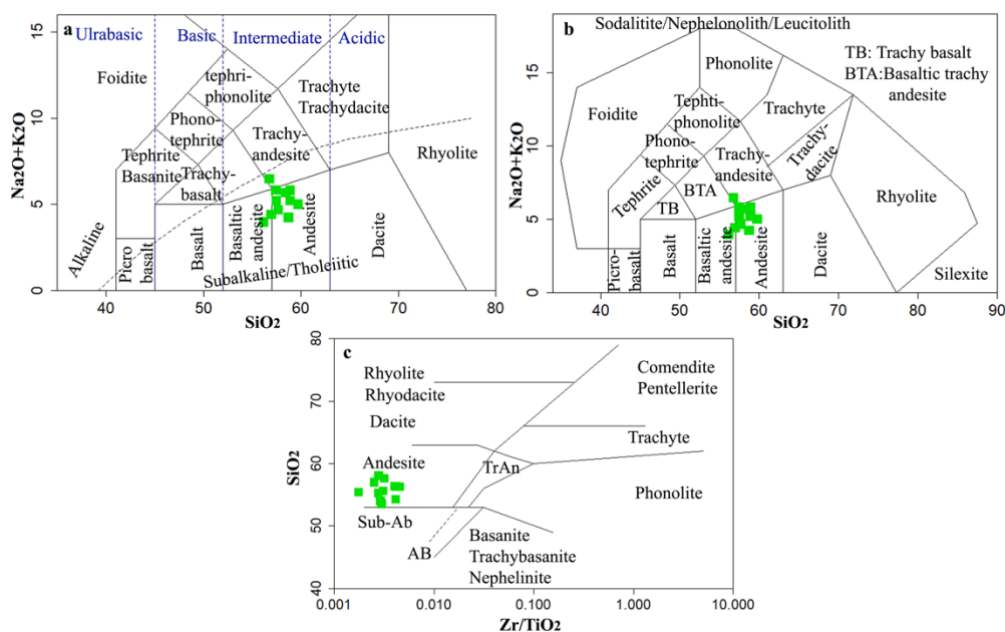


**Fig. 8.** Total alkali-silica diagrams of the Gallala volcanic rocks. a: Na<sub>2</sub>O+K<sub>2</sub>O vs. SiO<sub>2</sub> (Le Bas et al., 1992); and b: Na<sub>2</sub>O+K<sub>2</sub>O vs. SiO<sub>2</sub> (Middlemost, 1994). c: The log Zr/TiO<sub>2</sub> vs. SiO<sub>2</sub> in the wt.% diagram after Winchester and Floyd (1977). TrAn Trachy- Andesite; AB, Alkali basalt; Sub-AB, Sub-Alkali basalt

The volcanic rocks of the Gallala area were plotted on the AFM ternary diagram of the tholeiite, and calc-alkaline series (Irvine and Baragar, 1971); most samples fall towards the F (Total FeO) and M (MgO) apex within the sub-alkaline range, while few samples emerged in the tholeiite range, suggesting basic to intermediate volcanic rocks, as well as being further classified as representing calc-alkaline series (Fig. 9a).

Additionally, the studied rock samples were plotted on the tectonic discrimination diagrams, representing mostly ocean arcs in the La/Yb versus Nb/La diagram (Hollocher et al., 2012) (Fig. 9b). In addition, the Zr versus Ti diagram of Pearce (1982), and Ti versus V plot of Shervais (1982), used for indicating the tectonic environment of the Gallala volcanic rocks, demonstrate island arc lavas or island-arc tholeiite (IAT) (Figs. 9c, and d). Ali (2012), also concluded that the volcanic rocks of the Walsh-Naopurdan volcano-sedimentary group are representatives of magmatic series that occurred in environments associated with subduction. These magmatic series range from island arc tholeiite to later calc-alkaline and late alkaline domains.

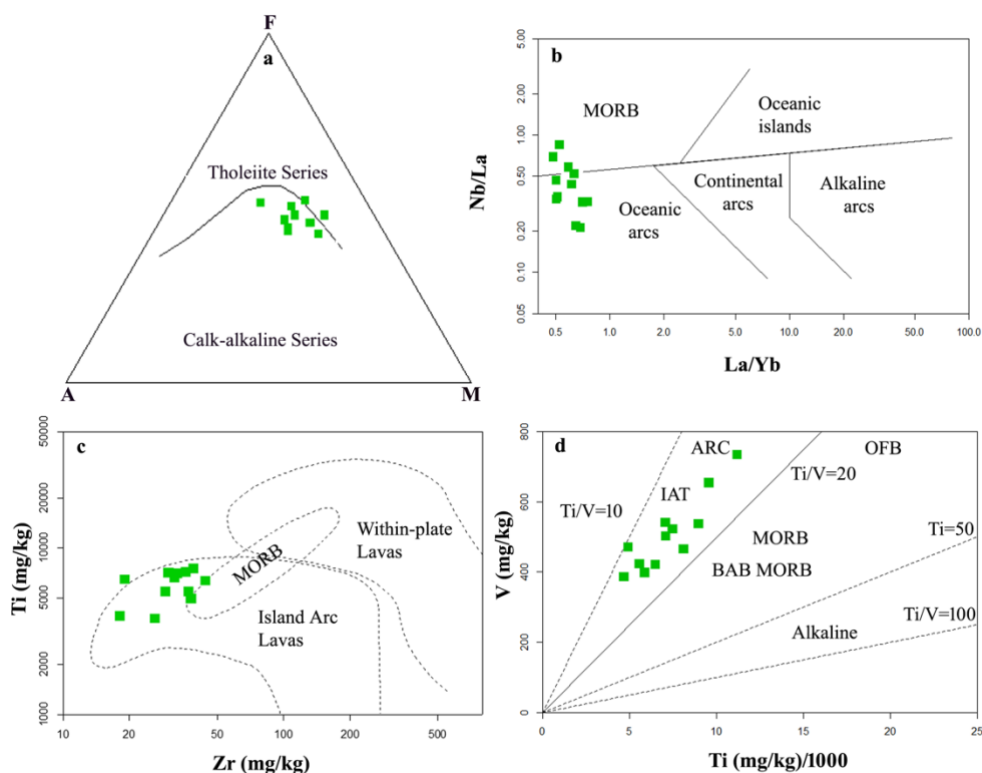


**Fig. 9.** The tectonic discrimination diagrams of the volcanic rocks of the Gallala area. a: The Ternary AFM diagram of Irvine and Baragar (1971). b: The La/Yb vs. Nb/La diagram (Hollocher et al., 2012). c: The Zr vs. Ti diagram (after Pearce (1982)). d: V vs. Ti/1000 for the Gallala samples, after Shervais (1982). IAT, Island-arc tholeiite; BAB, Back-arc basin basalt; MORB, Mid-Ocean ridge basalt; OFB, Ocean flood basalt

Some trace element abundances can be attributed to the influence of hydrothermal alteration of the volcanic rocks in the source area. One of the proper methods for characterizing magmatic transformation is the variation in minor elements relative to MgO. The Co, Ni, and Cr are predominant compatible elements in the Gallala volcanic rock samples. The positive correlation of chromium and cobalt with MgO coinciding with slight negative to the negative correlation of Ni and Y against magnesium oxides leads to inferring that the mafic minerals such as pyroxene and amphiboles have undergone hydrothermal alteration, producing actinolite and chlorite (Fig. 10). The crystallization process plays the key petrographical function in basaltic magma evolution in the Gallala area, as well as the scattering of traces concerning the major oxides can be attributed to mafic minerals and plagioclase phenocrysts (Sarem et al., 2021).

## 5.2. Mineralization Styles and Mineral Paragenesis

The sulfide mineralogy of the disseminated ore type is dominated by iron sulfides with a subordinate content of iron oxides. On the other hand, the main sulfide mineral of the massive vein ore types is pyrite, with a minor amount of chalcopyrite, bornite, covellite, sphalerite, and pyrrhotite. The most common gangue minerals in the studied samples are chlorite, albite, sericite, actinolite, epidote, and quartz

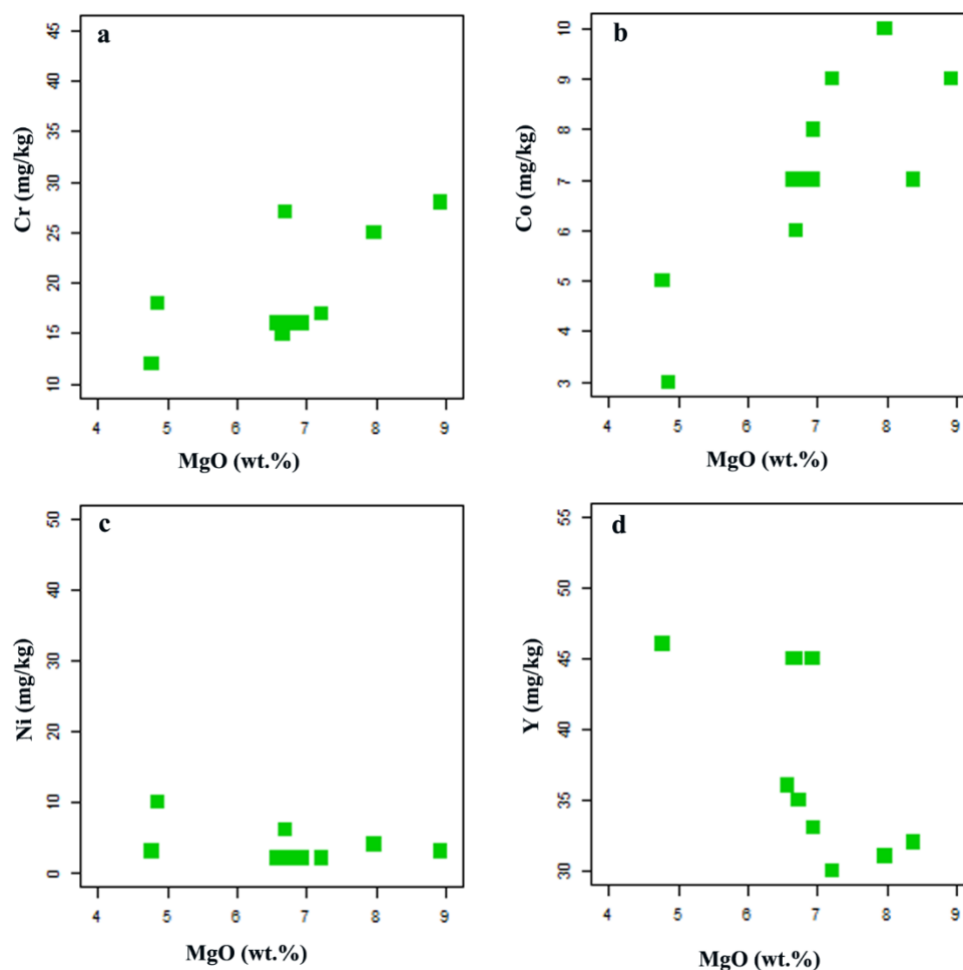


**Fig. 10.** a-d: Binary diagrams displaying major and trace elements variation of the Gallala host rocks

Deformed pyrites are the main pyritic generation that was recognized in the Gallala sulfide mineralization. Deformation and fracturing of the ore bodies occurred syn-genetically or epigenetically due to shearing resulting in the brecciated texture of the coarse pyrite grains (Craig et al., 1981, Pracejus, 2015, Awadh, 2006, Ramdohr, 2013) (Fig. 7fc).

Commonly, pyrite is replaced by Cu-sulfides, and later on by sphalerite, and covellite (Fig. 7 d, e, and f). The replacement of chalcopyrite by bornite occurs under hydrothermal conditions in solutions containing Cu and hydrosulfide over the temperature range 200-320 °C at autogenous pressures (Zhao et al., 2014) (Fig. 7 d, and e).

The mineral composition and their textural mutual relationships from the ore petrography indicate that several ingredients provided the formation of Gallala sulfide mineralization. The proposed formation processes are divided into two hydrothermal stages (Fig. 11). The paragenetic minerals originated from the hydrothermal fluids that produce the epigenetic to the volcanic rocks, ore minerals-filled veinlets, and fissures. The later exposed sulfide mineralization was affected by surface weathering that resulted in the alteration of the primary ore to secondary ore such as limonite, and malachite staining.

The studied samples were obviously distinguished by replacing earlier phases such as mafic minerals, while plagioclases like albite altered to sericite. Moreover, sericitization, chloritization, and epidotization are the dominant alteration of the host rocks. From the optical features, it is revealed that

the sericitization occurred from the alteration of plagioclase, whereas chloritization, and epidotization occurred by the alteration of mafic minerals. In addition, pyroxene in several cases is altered and replaced by hornblende. These observations lead to the conclusion that the volcanic rocks in the G-MVR region were affected by hydrothermal processes that resulted in alteration and resorption (Aswad et al., 2014) (Fig. 6d, f, and h).

The pre-stage of mineralization displays a minority of remnant silicate minerals observed in the host rocks. The oldest recognized minerals are composed of microphenocrysts of augite (clinopyroxene), a green anhedral crystal of hornblende (Fig. 6d), an equant quartz grains (Fig. 6f), and the laths shapes of plagioclase albite (Fig. 6j). The sulfide mineralization in the Gallala area occurred after the magmatic crystallization of the host rocks, as a result of hydrothermal alterations, during which Fe-sulfides formed.

The earliest stage of ore mineralization occurred, during the final stage of magma consolidation, and is represented by the formation of iron oxides (i.e., magnetite and pseudomorphs of hematite after magnetite) that progressively alter to pyrrhotite and pyrite, during interaction with more reductive aqueous solutions of volcanogenic to hydrothermal origin (Fig. 7 a, b, and c). Qian et al. (2010) proposed that magnetite was replaced by Fe-disulfides (i.e., pyrrhotite, and pyrite) under hydrothermal conditions. These solutions have traced the pathway from the source, and as a result of subsequent cooling and chemical reactions, they are eventually forced to deposit their load in cavities and fissures, therefore forming the observed vein structures.



**Fig. 11.** Paragenesis diagram of the ore and gangue minerals of the Gallala sulfide mineralization

The transition between the early to the late stage of hydrothermal sulfide mineralization is marked by the replacement of pyrite by chalcopyrite and bornite (Fig 7 d, e, and f). The chemical restrictions of the hydrothermal replacement are also displayed in Figure 7 h, in which the pyrite seems to be replaced by chalcopyrite to form a zonal texture. The zonal growth of pyrite and chalcopyrite was formed due to the chemical and temperature variations of the hydrothermal fluids (Pracejus, 2015).

The diversity of the sulfide mineral assemblages of the hydrothermal deposit minerals represents the main period of maturation from subhedral to anhedral pyrite crystals, with a minor amount of pyrrhotite, sphalerite, chalcopyrite inclusions (Fig. 7 c, d, e, and f); moreover, at the later stage of ore mineralization, a part of the anhedral chalcopyrite crystals seem to be replaced by covellite (Fig. 6d, e, and f). The well-preserved mineral growth and slow cooling along with high-temperature fluids give rise to form the euhedral coarse-grained pyrite in the Luoyangou gold deposit, which indicates that the origin of the sulfide minerals derived from the magmatic fluids, whereas, the fine-grained polymetallic

minerals were formed by association with meteoric water under changeable physiochemical conditions of the ore-forming fluids (Song et al., 2023). Generally, actinolite+chlorite+epidote+sericite minerals are the dominant secondary minerals that occur by the alteration of silicate minerals in the volcanic host rocks, which are associated with ore minerals (Fig.7). The post-mineralization stage is dominated by quartz, calcite, as well as malachite, and pseudomorphs of limonite on pyrite, which could be classified as supergene ores (Fig.11). Due to the mutual relative facts between mineralogical and paragenetical sequences of the sulfide mineralization indicate that their genesis occurred at a later stage than the formation of the host rock (volcanogenic to hydrothermal origin), this type of mineralization could also be categorized as epigenetic ores.

## 6. Conclusions

In the Gallala area, and within the Walash-Naopurdan Group of the Zagros Orogen about 150 km from Erbil city in the Kurdistan Region of Iraq, a volcanogenic-hydrothermal sulfide mineralization is reported for the first time.

The sulfide mineralization is hosted by intermediate volcanic rocks, including basaltic andesite and andesite with sub-alkaline to low-K tholeiitic character. The host rocks are mostly composed of clinopyroxene, hornblende, albite, sericite, actinolite, epidote, chlorite, quartz, and opaque minerals, pointing to sericitic and propylitic alteration effects.

The ore petrography demonstrates that the major ore mineral is pyrite, with subordinate occurrences of chalcopyrite, pyrrhotite, sphalerite, bornite, and covellite. Magnetite and hematite are the two iron oxides encountered only along the disseminated sulfides.

The overall petrographic characteristics indicate that the genesis of the sulfide mineralization took place mostly within the hydrothermal stages.

By applying geochemical indices, it is inferred that the geodynamic setting of host rocks of the Gallala sulfide mineralization fits the oceanic arc or island arc tholeiite suite.

## Acknowledgements

University of Patras, is acknowledged for the XRF analyses. Dr. Paraskevi Lampropoulou and Mr. Nikos Sofis Department of Geology University of Patras, are thanked for their contribution to the X-ray diffraction analysis and sample preparation. The authors have no competing interests to declare that are relevant to the content of this article.

## References

- Adamides, N., 2010, Mafic-dominated volcanogenic sulphide deposits in the Troodos ophiolite, Cyprus Part 2—A review of genetic models and guides for exploration: *Applied Earth Science*, 119(4), 193-204.
- Agard, P., Omrani, J., Jolivet, L., Whitechurch, H., Vrielynck, B., Spakman, W., Monié, P., Meyer, B., Wortel, R., 2011, Zagros orogeny: a subduction-dominated process: *Geological Magazine*, 148(5-6), 692-725.
- Ahmed, I. N., Kettanah, Y. A., Ismail, S. A., 2020, Genesis and tectonic setting of high-Cr podiform chromitites of the Rayat ophiolite in the Zagros Suture Zone, northeastern Iraq: *Ore Geology Reviews*, v. 123, 103583.
- Al-Bassam, K. S., 2013, Mineral resources of Kurdistan region, Iraq: *Iraqi Bulletin of Geology and Mining*, 9, 3, 103-127.
- Al-Chalabi, S., 2004, Mineralogy and origin of Chromate in Qalander area Northern Iraq: M. Sc. Thesis, Salahaddin University, Erbil, Iraq, 104.
- Alavi, M., Mahdavi, M., 1994, Stratigraphy and structures of the Nahavand region in western Iran, and their implications for the Zagros tectonics: *Geological Magazine*, 131, 1, 43-47.
- Ali, S. A., 2012, Geochemistry and geochronology of Tethyan-arc related igneous rocks, NE Iraq: *Research Online*, 390.

- Ali, S. A., Buckman, S., Aswad, K. J., Jones, B. G., Ismail, S. A., Nutman, A. P., 2013, The tectonic evolution of a Neo-Tethyan (Eocene–Oligocene) island-arc (Walash and Naopurdan groups) in the Kurdistan region of the Northeast Iraqi Zagros Suture Zone: *Island Arc*, 22(1), 104-125.
- Aswad, K. J., 1999, Arc-continent collision in Northeastern Iraq as evidenced by Mawat and Penjwin Ophiolite Complexes: *Raffidain Journal of Science*, 10, 51-61.
- Aswad, K. J., Al-Samman, A. H., Aziz, N. R., Koyi, A., 2014, The geochronology and petrogenesis of Walash volcanic rocks, Mawat nappes: constraints on the evolution of the northwestern Zagros suture zone, Kurdistan Region, Iraq: *Arabian Journal of Geosciences*, 7(4), 1403-1432.
- Aswad, K. J., Aziz, N. R., Koyi, H. A., 2011, Cr-spinel compositions in serpentinites and their implications for the petrotectonic history of the Zagros Suture Zone, Kurdistan Region, Iraq: *Geological Magazine*, 148(5-6), 802-818.
- Aswad, K. J., Elias, E., 1988, Petrogenesis, geochemistry and metamorphism of spilitized subvolcanic rocks of the Mawat Ophiolite Complex, NE Iraq: *Ofioliti*, 13(2/3), 95-109.
- Awadh, S. M., 2006, Mineralogy, geochemistry and origin of the zinc–lead–barite deposits from selected areas from north of Zakho, Northern Iraq: *Iraqi Journal of Science*, 119-131.
- Aziz, N. R., 2008, Petrogenesis, Evolution, and Tectonics of the Serpentinites of the Zagros Suture Zone, Kurdistan Region, NE Iraq: Ph.D. Thesis, 274.
- Badrzadeh, Z., Barrett, T. J., Peter, J. M., Gimeno, D., Sabzehei, M., and Aghazadeh, M., 2011, Geology, mineralogy, and sulfur isotope geochemistry of the Sargaz Cu–Zn volcanogenic massive sulfide deposit, Sanandaj–Sirjan Zone, Iran: *Mineralium Deposita*, 46(8), 905-923.
- Barber, D. E., Stockli, D. F., Horton, B. K., Koshnaw, R. I., 2018, Cenozoic exhumation and foreland basin evolution of the Zagros orogen during the Arabia-Eurasia collision, western Iran: *Tectonics*, 37(12), 4396-4420.
- Buday, T., 1980, The regional geology of Iraq: stratigraphy and paleogeography, Baghdad, State Organization for Minerals, Iraq Geological Survey, 445.
- Craig, J. R., Vaughan, D. J., Hagni, R. D., 1981, Ore microscopy and ore petrography, Wiley New York, 424.
- Eldridge, C. S., Barton, P. B., Ohmoto, H., 1983, Mineral textures and their bearing on formation of the Kuroko orebodies: *Economic Geology*, 241-281.
- Fouad, S. F., 2015, Tectonic map of Iraq, scale 1: 1000 000, 2012: *Iraqi Bulletin of Geology and Mining*, 11(1), 1-7.
- Haymon, R. M., Koski, R. A., Sinclair, C., 1984, Fossils of hydrothermal vent worms from Cretaceous sulfide ores of the Samail Ophiolite, Oman: *Science*, 223(4643), 1407-1409.
- Hollocher, K., Robinson, P., Walsh, E., Roberts, D., 2012, Geochemistry of amphibolite-facies volcanics and gabbros of the Støren Nappe in extensions west and southwest of Trondheim, Western Gneiss Region, Norway: a key to correlations and paleotectonic settings: *American Journal of Science*, 312(4), 357-416.
- Irvine, T. N., Baragar, W., 1971, A guide to the chemical classification of the common volcanic rocks: *Canadian Journal of Earth Sciences*, 8(5), 523-548.
- Ismail, S. A., Al-Chalabi, S. A., 2006, Genesis of Chromitite in Qalander Area, Northern Iraq Employing Cr-Rich Spinel: *Journal of Kirkuk University–Scientific Studies*, 1, 2.
- Ismail, S. A., Arai, S., Ahmed, A. H., Shimizu, Y., 2009, Chromitite and peridotite from Rayat, northeastern Iraq, as fragments of a Tethyan ophiolite: *Island Arc*, 18(1), 175-183.
- Ismail, S. A., Kettanah, Y. A., Chalabi, S. N., Ahmed, A. H., Arai, S., 2014, Petrogenesis and PGE distribution in the Al- and Cr-rich chromitites of the Qalander ophiolite, northeastern Iraq: Implications for the tectonic environment of the Iraqi Zagros Suture Zone: *Lithos*, 202, 21-36.
- Jassim, S. Z., Goff, J. C., 2006, *Geology of Iraq*, Dolin, sro, distributed by Geological Society of London, 337.
- Jassim, Z., Buda, G., Neuzilova, M., Suk, M., 1982, Metamorphic development of the Iraqi Zagros ophiolite zone: *Krystalinikum*, 16, 21-40.
- Koshnaw, R. I., Schlunegger, F., Stockli, D. F., 2021, Detrital zircon provenance record of the Zagros mountain building from the Neotethys obduction to the Arabia–Eurasia collision, NW Zagros fold–thrust belt, Kurdistan region of Iraq: *Solid Earth*, 12(11), 2479-2501.
- Le Bas, M., Le Maitre, R., Woolley, A., 1992, The construction of the total alkali-silica chemical classification of volcanic rocks: *Mineralogy and petrology*, 46(1), 1-22.

- Marshall, B., Gilligan, L., 1993, Remobilization, syn-tectonic processes and massive sulphide deposits: *Ore Geology Reviews*, 8(1-2), 39-64.
- Middlemost, E. A., 1994, Naming materials in the magma/igneous rock system: *Earth-science reviews*, 37(3-4), 215-224.
- Oudin, E., Constantinou, G., 1984, Black smoker chimney fragments in Cyprus sulphide deposits: *Nature*, 308(5957), 349-353.
- Palinkas, L. A., Mirza, T. A., 2020, Ridge-axis and Off-axis volcanic massive sulphide, Cyprus-type, in the Mawat Ophiolites, Kurdistan-Iraq, Reconnaissance survey: *Journal of Zankoy Sulaimani*, v, 103-122.
- Pearce, J. A., 1982, Trace element characteristics of lavas from destructive plate boundaries: *Orogenic andesites and related rocks*, 528-548.
- Pirouei, M., Kolo, K., Kalaitzidis, S. P., Abdullah, S. M., 2021, Newly discovered gossanite-like and sulfide ore bodies associated with microbial activity in the Zagros ophiolites from the Rayat area of NE Iraq: *Ore Geology Reviews*, 135, 104191.
- Pirouei, M., Kolo, K., Kalaitzidis, S. P., Sobhanverdy, J., 2022, Mapping of geochemical anomalies in the Zagros ophiolites stream sediments by fractal and classical analyses: implication for mineral exploration in Iraqi Kurdistan: *Arabian Journal of Geosciences*, 15(6), 1-18.
- Pracejus, B., 2015, *The ore minerals under the microscope: an optical guide*, Elsevier.
- Qian, G., Brugger, J., Skinner, W. M., Chen, G., Pring, A., 2010, An experimental study of the mechanism of the replacement of magnetite by pyrite up to 300 C: *Geochimica et Cosmochimica Acta*, 74 (19), 5610-5630.
- Ramdohr, P., 2013, *The ore minerals and their intergrowths*, Elsevier.
- Sarem, M. N., Abedini, M. V., Dabiri, R., Ansari, M. R., 2021, Geochemistry and petrogenesis of basic Paleogene volcanic rocks in Alamut region, Alborz mountain, north of Iran: *Earth Sciences Research Journal*, 25(2), 237-245.
- Shervais, J. W., 1982, Ti-V plots and the petrogenesis of modern and ophiolitic lavas: *Earth and planetary science letters*, 59(1), 101-118.
- Siavalas, G., Linou, M., Chatziapostolou, A., Kalaitzidis, S., Papaefthymiou, H., and Christanis, K., 2009, Palaeoenvironment of seam I in the Marathousa lignite mine, Megalopolis basin (Southern Greece): *International Journal of Coal Geology*, 78, 233-248.
- Simonov, V., Gaskov, I., Kovyazin, S., 2010, Physico-chemical parameters from melt inclusions for the formation of the massive sulfide deposits in the Altai-Sayan Region, Central Asia: *Australian Journal of Earth Sciences*, 57(6), 737-754.
- Slack, J. F., Foose, M. P., Flohr, M. J., Scully, M. V., Belkin, H. E., 2003, Exhalative and subsea-floor replacement processes in the formation of the Bald Mountain massive sulfide deposit, northern Maine.
- Song, F., Zhang, Q., Koua, K. A. D., Wu, H., Zhou, C., Wu, D., Sun, H., 2023, Trace Element and Sulfur Isotopic Analysis of Pyrite from the Luyuangou Gold Deposit, Xiong'ershan Au-Ag Polymetallic District, Central China: Implications for The Origin and Evolution of Ore-Forming Fluids: *Minerals*, 13(3), 407.
- Tyrrell, G. W., 2012, *The principles of petrology: an introduction to the science of rocks*, Springer Science & Business Media.
- Ural, M., Arslan, M., Göncüoğlu, M. C., Tekin, K. U., Kürüm, S., 2015, Late Cretaceous arc and back-arc formation within the Southern Neotethys: whole-rock, trace element and Sr-Nd-Pb isotopic data from basaltic rocks of the Yüksekova Complex (Malatya-Elazığ, SE Turkey): *Ofioliti*, 40, 1.
- Warr, L. N., 2021, IMA-CNMNC approved mineral symbols: *Mineralogical Magazine*, 85(3), 291-320.
- Winchester, J. A., Floyd, P. A., 1977, Geochemical discrimination of different magma series and their differentiation products using immobile elements: *Chemical Geology*, 20, 325-343.
- Zainy, M., Al-Ansari, N., Bauer, T., Ask, M., 2017, The tectonic and structural classifications of the Western part of the Zagros Fold and Thrust Belt, North Iraq, review and discussion: *Journal of Earth Sciences and Geotechnical Engineering*, 7(2), 71-89.
- Zhang, Z., Xiao, W., Majidifard, M. R., Zhu, R., Wan, B., Ao, S., Chen, L., Rezaeian, M., Esmaili, R., 2017, Detrital zircon provenance analysis in the Zagros Orogen, SW Iran: implications for the amalgamation history of the Neo-Tethys: *International Journal of Earth Sciences*, 106(4), 1223-1238.
- Zhao, J., Brugger, J., Ngothai, Y., Pring, A., 2014, The replacement of chalcopyrite by bornite under hydrothermal conditions: *American Mineralogist*, 99(11-12), 2389-2397.